Structure of the Bacteriophage λ Ser/Thr Protein Phosphatase with Sulfate Ion Bound in Two Coordination Modes[†,‡]

Walter C. Voegtli,[§] Daniel J. White,[||] Nicholas J. Reiter,[||] Frank Rusnak,[||] and Amy C. Rosenzweig*[,§]

Departments of Biochemistry, Molecular Biology and Cell Biology and of Chemistry, Northwestern University, Evanston, Illinois 60208, and Section of Hematology Research and the Department of Biochemistry and Molecular Biology, Mayo Clinic and Foundation, Rochester, Minnesota 55905

Received September 6, 2000; Revised Manuscript Received October 23, 2000

ABSTRACT: The protein phosphatase encoded by bacteriophage λ (λPP) belongs to a family of Ser/Thr phosphatases (Ser/Thr PPases) that includes the eukaryotic protein phosphatases 1 (PP1), 2A (PP2A), and 2B (calcineurin). These Ser/Thr PPases and the related purple acid phosphatases (PAPs) contain a conserved phosphoesterase sequence motif that binds a dinuclear metal center. The mechanisms of phosphoester hydrolysis by these enzymes are beginning to be unraveled. To utilize λPP more effectively as a model for probing the catalytic mechanism of the Ser/Thr PPases, we have determined its crystal structure to 2.15 Å resolution. The overall fold resembles that of PP1 and calcineurin, including a conserved βαβαβ structure that comprises the phosphoesterase motif. Substrates and inhibitors probably bind in a narrow surface groove that houses the active site dinuclear Mn(II) center. The arrangement of metal ligands is similar to that in PP1, calcineurin, and PAP, and a bound sulfate ion is present in two novel coordination modes. In two of the three molecules in the crystallographic asymmetric unit, sulfate is coordinated to Mn2 in a monodentate, terminal fashion, and the two Mn(II) ions are bridged by a solvent molecule. Two additional solvent molecules are coordinated to Mn1. In the third molecule, the sulfate ion is triply coordinated to the metal center with one oxygen coordinated to both Mn(II) ions, one oxygen coordinated to Mn1, and one oxygen coordinated to Mn2. The sulfate in this coordination mode displaces the bridging ligand and one of the terminal solvent ligands. In both sulfate coordination modes, the sulfate ion is stabilized by hydrogen bonding interactions with conserved arginine residues, Arg 53 and Arg 162. The two different active site structures provide models for intermediates in phosphoester hydrolysis and suggest specific mechanistic roles for conserved residues.

Reversible phosphorylation of proteins is an essential mechanism for signal transduction and metabolic regulation in all organisms (*1*, *2*). Protein phosphorylation by kinases occurs primarily on tyrosine, serine, and threonine residues (*3*, *4*). Protein phosphatases (PPases),[1] which can be conveniently divided into two classes based on substrate specificity, are responsible for their dephosphorylation (*5*, *6*). Removal of phosphoryl groups from phosphotyrosine substrates is catalyzed by protein tyrosine phosphatases (PTPases) (*7*), and phosphoserine/threonine substrates are hydrolyzed specifically by serine/threonine phosphatases (Ser/Thr PPases) (*8*). A subfamily of dual-specificity PTPases can dephosphorylate phosphoserine/threonine as well (*5*). Ser/Thr PPases are involved in crucial cellular processes, including gene expression, cell growth, and cell differentiation. Numerous pathophysiological conditions have been attributed to aberrant regulation of these enzymes including cancer, cardiac hypertrophy, immunosuppression, and apoptosis (*9*−*11*).

The eukaryotic Ser/Thr PPases utilize a dinuclear metal cluster for catalysis whereas no metal ions are required by PTPases. On the basis of amino acid sequences of their catalytic domains, the Ser/Thr PPases fall into two structurally distinct families. Using nomenclature for human genes, the symbol PPP has been chosen to represent the family that includes protein phosphatases 1 (PP1), 2A (PP2A), and 2B (PP2B or calcineurin), whereas PPM has been selected to represent the evolutionarily distinct family that includes protein phosphatase 2C (PP2C) and related enzymes (*12*). PP1, PP2A, and calcineurin share a conserved phosphoesterase sequence motif, $DXH(X)_nGDXXDR(X)_nGNHE$, where n is ∼25 residues (*13*−*15*). The X-ray structures of PP1 (*16*, *17*) and calcineurin (*18*, *19*) revealed that this phosphoesterase motif forms a βαβαβ substructure that provides four of the six ligands to the dinuclear metal center

[†] This work was supported by funds from the Robert H. Lurie Cancer Center at Northwestern University (A.C.R.) and by NIH Grant GM46864 (to F.R.) W.C.V. is supported in part by NIH Training Grant GM08382-10.

[‡] Refined coordinates have been deposited in the Protein Data Bank with accession code 1G5B.

* Address correspondence to this author. Telephone: (847)467-5301. Fax: (847)467-6489. E-mail: amyr@northwestern.edu.

[§] Northwestern University.

[||] Mayo Clinic and Foundation.

[1] Abbreviations: PPase, protein phosphatase; PTPase, protein tyrosine phosphatase; Ser/Thr PPase, serine/threonine phosphatase; PP1, protein phosphatase 1; PP2A, protein phosphatase 2A.; PP2B, protein phosphatase 2B (calcineurin); PP2C, protein phosphatase 2C.; PAP, purple acid phosphatase; λPP, bacteriophage λ protein phosphatase; EPR, electron paramagnetic resonance; EMTS, sodium ethylmercurithiosalicylate; MAD, multiwavelength anomalous dispersion; rms, root mean square.

10.1021/bi0021030 CCC: $19.00
Published on Web 11/23/2000

(*20*). Calcineurin and PP1 also exhibit a common catalytic domain topology that generates the substrate binding groove and active site cavity.

The phosphoesterase motif observed in the eukaryotic Ser/Thr PPases is conserved in a number of other enzymes involved in the hydrolysis of phosphate esters (*15*), including the purple acid phosphatases (PAPs) (*21*) and a protein phosphatase encoded by bacteriophage λ (λPP) (*14*, *22*). In the purple acid phosphatases, this motif also forms a $\beta\alpha\beta\alpha\beta$ fold at the core of the catalytic domain (*23*−*26*). The active sites of PP1, calcineurin, and PAP are composed of two metal ions separated by 3−4 Å. The identities of these metal ions in PPases under physiological conditions have not been conclusively established. Although different combinations of metal ions have been observed or assigned in the crystal structures, including Fe(III)Fe(II) (*25*, *26*), Fe(III)Zn(II) (*18*, *19*, *24*), and Fe(III)Mn(II) (*17*), the coordination geometries at the active sites are similar. In all three enzymes, the two metal ions are linked by a bridging solvent molecule and a μ-1,1 aspartic acid. Additional ligands include a histidine and an aspartic acid to the first metal ion and two histidines and an asparagine to the second metal ion. The locations of other conserved residues in the phosphoesterase motif are also similar. A distinguishing feature of the PAPs is the presence of a coordinated tyrosine, which is responsible for the purple color of PAPs due to a phenolate-to-Fe(III) charge-transfer transition (*21*). The similarities in sequence, fold, and active site structure of these enzymes suggest that the mechanism of phosphoester hydrolysis is conserved in this class of phosphoesterases.

One of the smallest members of this enzyme family is λPP (*27*) with 221 amino acid residues as compared to 330 for PP1 and 524 for the calcineurin catalytic subunit. Residues 15−144 of λPP are homologous to the N-terminal regions of the PP1 and calcineurin catalytic domains, and all the conserved residues in the phosphoesterase motif are present (*22*). The ability to generate large quantities of purified λPP combined with its smaller size have led to its use as a model system for studying the structure and function of Ser/Thr PPases. Initial studies indicated that λPP can utilize several divalent metal ions for catalysis, but the two that yield the highest activity are Mn(II) and Ni(II) (*22*). The formation of an exchange-coupled dinuclear Mn(II) cluster has been demonstrated recently by electron paramagnetic resonance (EPR) spectroscopy (*28*). In addition, λPP can be reconstituted with iron to form an Fe(III)Fe(II) cluster (*29*) spectroscopically similar to those observed in calcineurin (*30*) and PAP (*21*). Site-directed mutagenesis studies have indicated that residues in the λPP phosphoesterase motif are important for metal binding, substrate binding, and catalysis (*14*, *29*). Comparable results were obtained for PP1 (*31*, *32*), supporting the notion that the catalytic mechanisms of λPP and its eukaryotic relatives are similar. By contrast, λPP is not inhibited by okadaic acid and microcystin (*22*), potent inhibitors of PP1 (*33*), and is therefore not a useful model for the regulation of eukaryotic Ser/Thr PPases. To provide a structural basis for these observed similarities and differences and to utilize λPP more effectively as a model for probing the catalytic mechanism of the Ser/Thr PPases, we have determined its structure to 2.15-Å resolution.

EXPERIMENTAL PROCEDURES

Purification of λPP for Crystallization. A plasmid pT7−7 derivative carrying the wild-type λPP DNA sequence was used to transform *Escherichia coli* strain BL21(DE3) for protein overexpression by the T7 system (*34*). Large-scale cultures were prepared by inoculating 5 mL of Luria broth containing 400 μg/mL ampicillin with single colonies from a plate of freshly transformed cells. These were grown at 37 °C to an optical density at 600 nm of 0.1, after which a 100-μL aliquot was used to inoculate another 5 mL of medium. At an optical density at 600 nm of 1.0, the 5 mL of culture was used to inoculate 100 mL of starter cultures. The 100-mL cultures were then used to inoculate large-scale cultures in 6-L Erlenmeyer flasks containing 1.5−2.0 L 2xTY and 400 μg/mL ampicillin. After induction with 0.3 mM IPTG at an optical density at 600 nm of 0.7−1.0, the temperature was lowered to 23 °C. Optical densities were measured with a Varian Cary 1 dual-beam spectrophotometer. Cells were harvested after 12−20 h by centrifugation at 1500*g* and resuspended in 25 mM Tris (pH 7.8), 2.0 mM EDTA, and 20% glycerol. Cells were lysed and homogenized in an ice-cooled Bead Beater (Biospec Products, Inc., Barlesville, OK) using 0.5-mm zirconia/silica beads with ten 10-s bursts of vortexing over 10 min to prevent overheating. After the cell extract was centrifuged at 40000*g* for 2 h, the supernatant was applied to a 250-mL column of DEAE Sephadex CL-6B (Pharmacia) equilibrated in 25 mM Tris (pH 7.8) and 2.0 mM EDTA. The column was washed with 3 vol of the same buffer, and λPP was eluted with 25 mM Tris (pH 7.8), 0.1 M NaCl, and 2.0 mM EDTA. Fractions containing the majority of the phosphatase activity were pooled, NaCl was added to 0.5 M, and the fractions were applied to a 100-mL phenyl Sepharose column (Pharmacia) equilibrated in 25 mM Tris (pH 7.8) and 0.5 M NaCl. This column was washed with 3 vol of the equilibration buffer and 3 vol of 25 mM Tris (pH 7.8), and λPP was eluted with 25 mM Tris (pH 7.8) containing 50% glycerol. The purest fractions as determined by SDS−PAGE were pooled and dialyzed twice against 4 L of 9 mM Tris (pH 7.8), 10% glycerol, and 1 mM DTT. The purified material was then further concentrated to 19−56 mg/mL using a YM-10 ultrafiltration membrane in a Diaflow cell (Amicon). All purification procedures were performed at 4 °C.

Crystallization and Data Collection. Protein precipitation observed in samples of λPP concentrated to 19−30 mg/mL was partially prevented by increasing the DTT concentration to 10 mM, suggesting that a reactive cysteine on the protein surface might be causing aggregation. To address this problem, 1 mM ethylmercurithiosalicylate (EMTS), a thiol-specific mercury compound, was added to the protein samples from a 50 mM stock solution. EMTS-treated samples were incubated at 4 °C for at least 12 h prior to crystallization trials, and no precipitation was observed. Crystals of λPP were grown by using the hanging drop vapor diffusion technique, in which 1-μL drops of protein solution at 19−30 mg/mL were mixed with 1 μL of precipitant solution and suspended over a 1-mL reservoir of precipitant solution. Initial small crystals were obtained at room temperature with a precipitant solution composed of 100 mM MES (pH 6.0), 350 mM ammonium sulfate, 20% PEG 4000, 100 mM ammonium acetate, 10 mM $MnCl_2$, and 20 mM DTT. These

Table 1: Data Collection and Refinement Statistics

	λ1	λ2	λ3	high resolution
		Data Collection[a]		
wavelength (Å)	1.0247	1.0098	0.99188	0.99188
resolution range (Å)	30.0−2.5	30.0−2.5	30.0−2.5	50.0−2.15
unique observations	39 237	39 145	39 243	61 405
total observations	573 488	572 458	574 288	435 477
completeness (%)	99.5 (100)	99.5 (100)	99.5 (100)	99.5 (99.6)
R_{sym}[b]	0.052 (0.132)	0.050 (0.136)	0.053 (0.143)	0.053 (0.316)
$\langle I/\sigma \rangle$	13.5 (6.6)	10.9 (6.1)	12.1 (6.0)	10.6 (2.4)
R_{cullis}[c]	0.75	0.78	0.71	
phasing power[d]	1.29	1.19	1.47	
		Refinement		
resolution range			50.0−2.15	
no. of reflections			57 583	
R-factor[e]			0.202	
R-free			0.228	
no. of protein, nonhydrogen atoms			5 316	
no. of nonprotein atoms			333	
rms bond length (Å)			0.006	
rms bond angles (°)			1.2	
average *B* value (Å^2)				
main chain			39.31	
side chain			43.21	

[a] All data collected at −160 °C using a 2K × 2K Mar CCD detector at the DND-CAT beamline at the Advanced Photon Source. Values in parentheses are for the highest resolution shells: 2.54−2.50 Å for λ1, λ2, λ3 and 2.19−2.15 Å for the high-resolution data. [b] $R_{sym} = \Sigma|I_{obs} - I_{avg}|/\Sigma I_{obs}$, where the summation is over all reflections. [c] R_{cullis} = lack of closure error/iso-ano difference (generalized R_{cullis} from CNS). [d] Phasing power = heavy atom structure factor/rms lack of closure error (statistics from CNS). [e] *R*-factor $= \Sigma|F_{obs} - F_{calc}|/\Sigma F_{obs}$. Five percent of the reflections were reserved for calculation of *R*-free.

crystals grew in 3−7 days and diffracted to 2.7 Å resolution. To improve crystal size and diffraction quality, a microcrystalline suspension was prepared by crushing 5−10 single crystals in 750 μL of precipitant solution and was used to streak new hanging drops with a cat whisker. Large triangular prismatic crystals, 0.5 mm in the longest dimension, appeared in a small percentage of these drops overnight. Crystals for data collection were soaked for 5−10 min in precipitant solution without DTT and with 20% glycerol as a cryosolvent, mounted in rayon loops, and flash cooled at −160 °C. All data were collected at the Dupont-Northwestern-Dow Collaborative Access Team (DND-CAT) beamline at the Advanced Photon Source using a 2K × 2K Mar CCD detector. Patterson analysis of data from a single wavelength anomalous scattering experiment indicated the presence of mercury in the crystal, and a multiwavelength anomalous dispersion (MAD) experiment was performed (Table 1). The data were processed with DENZO and SCALEPACK (*35*). The crystals belong to the space group $C222_1$ with unit cell dimensions $a = 160.4$, $b = 177.3$, and $c = 79.1$ Å.

Structure Determination. Two mercury sites were located by Patterson analysis using the CCP4 suite of programs (*36*) and by direct methods using SHELX (*37*). MAD phasing and density modification with CNS (*38*) yielded an electron density map in which a number of α helices were apparent. The program O (*39*) was used to build models of two molecules in the asymmetric unit, and the position of a third was determined by molecular replacement with AmoRe (*36*) using the coordinates of a previously built molecule as the search model. The three molecules are designated molecules A−C. Iterative cycles of rigid body, positional, simulated annealing, and individual *B*-value refinement with CNS (*38*) followed by model rebuilding with O (*39*) were conducted using the free *R*-value to monitor the refinement progress. Three pairs of large peaks (>8σ) separated by ∼3.5 Å in $F_o - F_c$ difference electron density maps were assigned as 6 Mn(II) ions since the crystallization solution contained 10 mM $MnCl_2$ and λPP is known to bind a pair of Mn(II) ions as a cofactor (*22*, *28*). Three peaks (>11σ) adjacent to the dimanganese clusters were assigned as sulfate ions based on the shape of the electron density and the presence of 350 mM ammonium sulfate in the crystallization buffer. Two additional sulfate ions were modeled into peaks at protein−protein contacts in the crystal lattice. The two mercury sites are located adjacent to Cys 208 in two of the three protein molecules (molecules A and B). Water molecules placed at peaks >3σ in $F_o - F_c$ difference electron density maps were retained if their refined *B*-values remained <60 Å^2. Noncrystallographic symmetry restraints were imposed until the final cycles of refinement to 2.15 Å resolution. The final model consists of all 221 residues for molecules B and C and residues 1−219 for molecule A. Ramachandran plots generated with PROCHECK (*40*) indicate that the model exhibits good geometry with 87.0% of the residues in the most favored regions and 10.7% in the favored and allowed regions. Three residues near the active site, Asp 52, Arg 53, and His 186, fall in disallowed regions in all three protein molecules. The homologous residues in PP1 (*16*) and calcineurin (*18*, *19*) adopt similar disallowed conformations as does the homologous histidine in PAP (*24*, *25*). Both Asp 52 and Arg 53 are linked to the dinuclear Mn(II) cluster by hydrogen bonds, and His 186 is coordinated to one of the Mn(II) ions. The carbonyl oxygen atom of His 186 is hydrogen bonded to a bridging solvent ligand. Figures were generated using MOLSCRIPT (*41*), RASTER3D (*42*), GRASP (*43*), and BOBSCRIPT (*44*).

RESULTS AND DISCUSSION

Overall Structure. λPP is a crescent shaped molecule with dimensions of 50 Å × 30 Å × 25 Å. The overall structure comprises two β sheets (4- and 6-stranded) and 6 α helices (Figure 1a,b). The $DXH(X)_nGDXXDR(X)_nGNHE$ phospho-

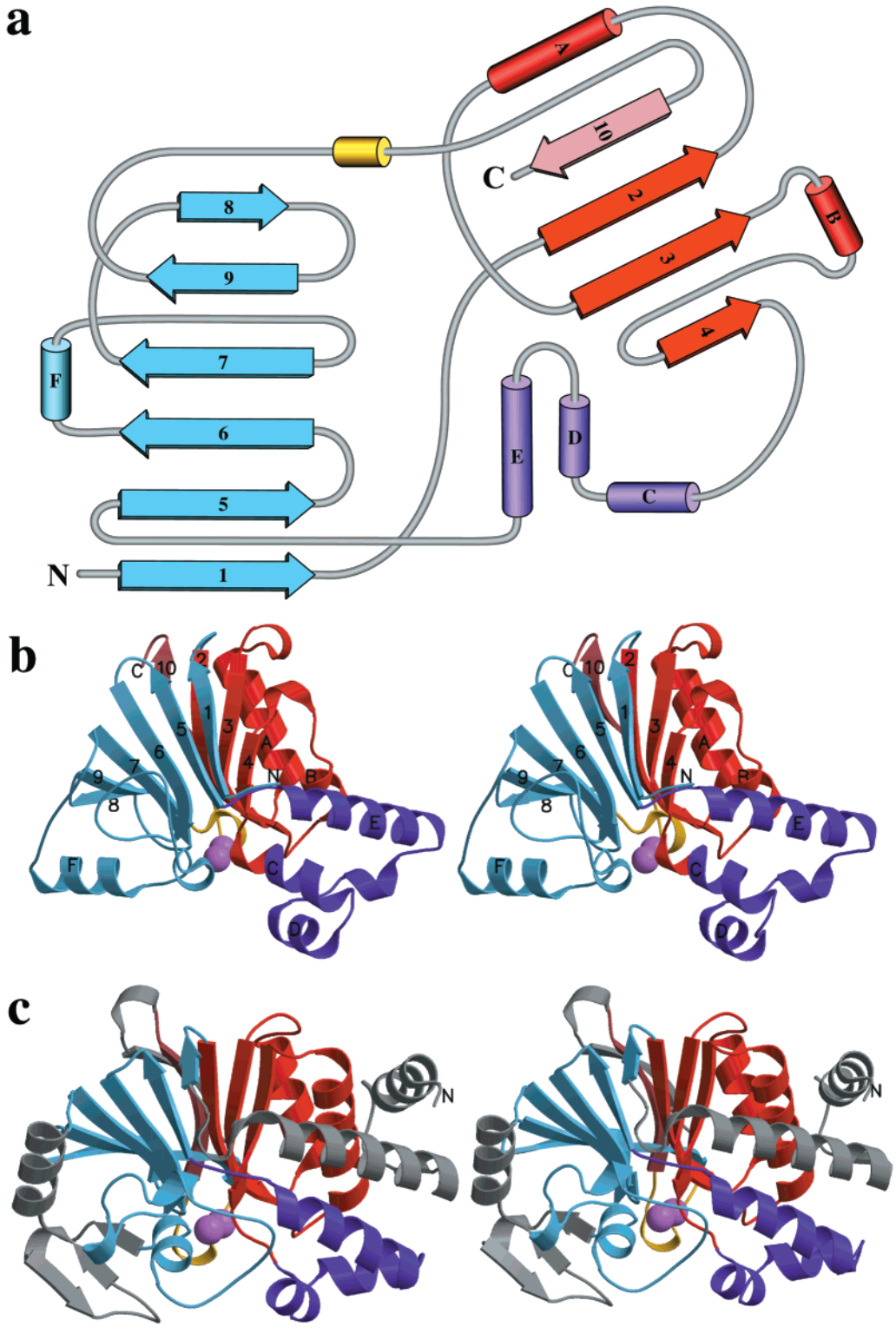

FIGURE 1: (a) Secondary structure diagram of λPP. α helices are shown as cylinders, and β strands are shown as arrows. Secondary structure assignments: β1, residues 3−9; β2, residues 14−22; β3, residues 42−51; β4, residues 70−73; β5, residues 124−130; β6, residues 133−140; β7, residues 180−186; β8, residues 192−195; β9, residues 197−201; β10, residues 213-218; αA, residues 24−36; αB, residues 57−62; αC, residues 74−84; αD, residues 90−97; αE, residues 106−122; αF, residues 162−171. The conserved phosphoesterase motif is shown in red. The helical turn and loop connecting β9 and β10 (residues 201−213) is shown in yellow. (b) Stereo ribbon diagram of λPP colored the same as in panel a. The 2 Mn(II) ions are shown as dark pink spheres. (c) Stereo ribbon diagram of rabbit PP1 (PDB accession code 1FJM). Secondary structure elements present in λPP are colored as in panels a and b. Secondary structure elements not present in λPP are shown in gray. The two metal ions are shown as dark pink spheres.

esterase motif is located within the N-terminus, spanning residues 15−77, and forms a βαβαβ structure that includes β2, β3, β4, αA, αB, and the N terminal region of αC. The conserved residues are positioned at the C-termini of β2 (residues Asp 20 and His 22) and β3 (Gly 48 and Asp 49) and at the N-terminus of αC (residues Gly 74, Asn 75, His 76, and Glu 77). The 4-stranded β sheet comprises the three β strands in the βαβαβ phosphoesterase motif and β10 from the C-terminus. The 6-stranded β sheet consists of strands β5, β6, β7, β8, β9, and β1 from the N-terminus. These

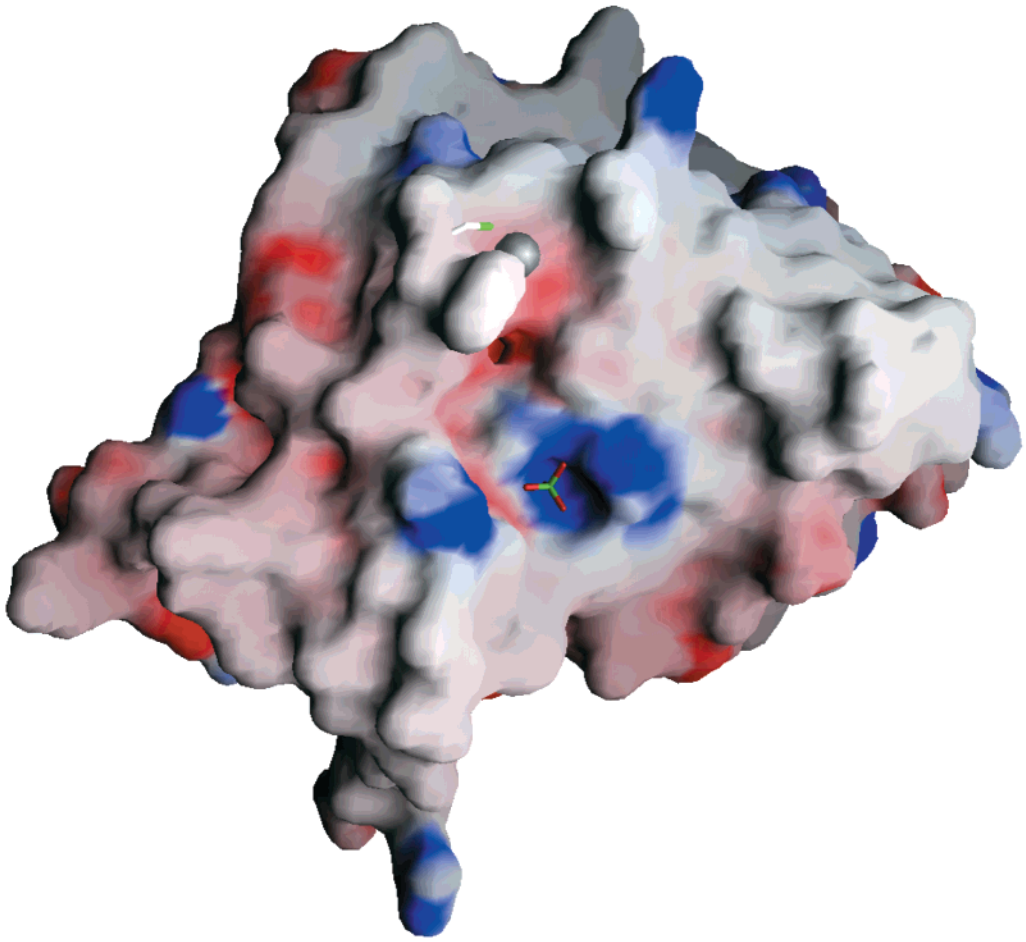

FIGURE 2: Surface representation of λPP molecule A colored according to electrostatic potential: red, −20 kT; white 0 kT; blue, +20 kT. The surface groove extends vertically in the plane of the page (bottom surface of the orientation shown in Figure 1b). A sulfate ion is bound to the dimanganese cluster in the active site cavity (sulfur atom in green and oxygen atoms in red). Two arginine residues, Arg 53 on the left and Arg 162 on the right, which in this figure are responsible for the central region of positive electrostatic potential surrounding the active site, interact with the bound sulfate ion. In molecules A and B, the surface groove also houses a Hg(II) ion (gray sphere) coordinated by Cys 208 (sulfur atom in green). The Hg(II) ion is partially covered by Phe 207.

features as well as three helices directly following the βαβαβ motif (αC, αD, and αE) are conserved in the structure of PP1 (Figure 1c). However, the smaller λPP is a simpler structure, lacking the N-terminal 50 residues of PP1 as well as a 3-stranded β sheet and an additional helix formed by PP1 residues 207−240 (*16*, *17*). In addition, the β sheet encompassing the three β strands in the PP1 βαβαβ motif is 5-stranded rather than 4-stranded as in λPP. The overall fold of λPP also resembles that of calcineurin (*18*, *19*), which is very similar to PP1. Since the entire λPP fold is conserved in its eukaryotic relatives, the λPP structure represents a minimal structural motif characteristic of the Ser/Thr PPase family.

A narrow, curved groove, ∼17 Å long and ∼4−8 Å wide, lies along the flatter surface of λPP (Figure 2). This groove houses the catalytic center and is probably the protein substrate and inhibitor binding site. The walls of the groove are formed by αC, αD, and the loop connecting β3 and αB on one side and by the helical turn just before αF, the loop connecting β7 and β8, and the helical turn formed by residues 205−209 on the other side (Figure 1b). The dinuclear manganese(II) cluster is located in the deepest part of the groove (Figures 1b and 2). The active site is formed by the two Mn(II) ions, residues Asp 20, His 22, Asp 49, Asp 52, Arg 53, Asn 75, and His 76 from the βαβαβ phosphoesterase motif substructure and residues His 139, His 186, and Asp 202 located on loops at the C-termini of β6, β7, and β9, respectively. An additional arginine residue, Arg 162, extends into the active site from its position on α6. In all three λPP molecules in the asymmetric unit, a sulfate ion is bound at the active site. The region of the groove adjacent to the active site contains a number of hydrophobic residues, including Pro 188, Ala 189, Val 190, Gly 204, and Phe 207. A mercury ion derived from EMTS added to the protein prior to crystallization is bound to Cys 208 in this part of the groove in molecules A and B (Figure 2). The section of the groove between the mercury binding site and the active site is negatively charged due to the presence of Asp 202 and could be important for recognition of substrates containing lysine and arginine residues.

A larger, Y-shaped surface groove is observed in the structure of PP1 (*16*, *17*). The three branches of this groove are termed the hydrophobic groove, the acidic groove, and the C-terminal groove and come together at the active site. The acidic and C-terminal grooves form the top part of the Y structure and are divided by a loop connecting PP1 strands β12 and β13 (analogous to λPP strands β9 and β10, yellow in Figure 1b,c). The acidic groove has been proposed to interact with the positively charged substrate DARRP-32 (*16*). The PP1 hydrophobic and acidic grooves are conserved

Table 2: Interatomic Distances in λPP Active Site

		distance (Å)		
	atom	molecule A	molecule B	molecule C
Mn1	Mn2	3.5	3.5	3.4
Mn1	Asp 20 Oδ2	2.4	2.2	2.2
Mn1	His 22 Nϵ2	2.2	2.2	2.2
Mn1	Asp 49 Oδ2	2.2	2.2	2.4
Mn1	SO_4^{2-} O1	−	−	2.1
Mn1	SO_4^{2-} O3	−	−	2.6
Mn1	W1	2.1	2.2	-
Mn1	W2	2.3	2.3	2.2
Mn1	W3	2.6	2.4	−
Mn2	Asp 49 Oδ2	2.3	2.4	2.2
Mn2	Asn 75 Oδ1	2.1	2.2	2.1
Mn2	His 139 Nϵ2	2.2	2.2	2.2
Mn2	His 186 Nδ1	2.2	2.2	2.3
Mn2	SO_4^{2-} O1			2.4
Mn2	SO_4^{2-} O2	2.4	2.3	2.4
Mn2	W1	2.3	2.4	

in λPP, but λPP lacks a region similar to the PP1 C-terminal groove. This groove in PP1 is formed by one side of the loop connecting β12 and β13 and residues near the N-terminus, which are not conserved in λPP. The β12-β13 loop is the site of microcystin and okadaic acid sensitivity in PP1, and the homologous loop is the site of cyclosporin/cyclophilin sensitivity in calcineurin (*16*, *17*). Differences in the structure of the corresponding β9−β10 loop in λPP combined with the absence of a groove corresponding to the PP1 C-terminal groove explain why λPP is not affected by these inhibitors (*22*). Interestingly, the N-terminal residues involved in the PP1 C-terminal groove are partly conserved in an archaeal protein phosphatase that is inhibited by these toxins (*45*).

Active Site Structure. The active site of λPP is shown in Figures 3−6. Protein ligands to the dimanganese cluster include four of the conserved residues in the phosphoesterase motif and two histidines from the C-terminal part of the protein. The two Mn(II) ions are separated by an average distance of 3.5 Å (Table 2). Mn1 is coordinated by the ϵ nitrogen of His 22 and by a single carboxylate oxygen atom of Asp 20. The uncoordinated side chain oxygen atom of Asp 20 is hydrogen bonded to the amide nitrogen of His 186. Mn2 is coordinated by the ϵ nitrogen of His 139, the δ nitrogen of His 186, and the amido oxygen of Asn 75. The Asn 75 coordinating atom was assigned as the oxygen since the amido group is likely to be protonated at physiologically relevant pH (*46*), and this is the preferred coordination mode in a number of model compounds (*47*). Asp 49 is coordinated to both Mn(II) atoms in a μ-1,1 fashion, with its uncoordinated side chain oxygen atom hydrogen bonded to the amide nitrogen of His 76. This arrangement of protein ligands, including hydrogen bonding interactions, is nearly identical to that observed in PP1 and calcineurin (*15*). Although His 139 and His 186 are not part of the phosphoesterase motif, their counterparts in PP1 and calcineurin derive from structurally conserved regions, supporting the notion that λPP comprises a minimal structural motif for this family.

The λPP active site also contains exogenous ligands, including a bound sulfate ion and several solvent molecules. In molecules A and B, the sulfate ion adopts a terminal, monodentate coordination mode to Mn2 with an average Mn···O distance of 2.35 Å (Figure 3, Table 2). Although several structures of phosphatases complexed with phosphate or tungstate are available (*17*, *18*, *24*−*26*), the λPP structure is the first in which a terminal coordination mode is observed. In these two molecules, the dimanganese cluster is bridged by a solvent molecule (W1), with average bond distances of 2.15 Å to Mn1 and 2.35 Å to Mn2. W1 is hydrogen bonded to the sulfate ion and to the carbonyl oxygen atom of His186. Two additional water or hydroxide ligands, W2 and W3, are coordinated to Mn1, with average Mn···O distances of 2.3 and 2.5 Å, respectively. W2, which is also present in molecule C, is hydrogen bonded to Asp 202. Thus, both Mn(II) ions are six-coordinate with distorted octahedral geometry. Some or all of these solvent molecules are also present in PP1, calcineurin, and PAP (*15*). The bridging solvent molecule has been assigned as hydroxide in PAP based on spectroscopic data (*24*, *25*). Assignment of the analogous ligand in λPP as hydroxide and the two terminal solvent molecules as water would render the overall active site charge neutral. According to EPR spectroscopic data, however, the dimanganese cluster exhibits a weak exchange interaction, which may indicate the presence of a μH_2O ligand (*28*). In addition, the Mn···μO distances are more consistent with a water bridge (*48*, *49*). Similar reasoning has been applied to the dimanganese enzyme arginase (*50*).

The bound sulfate ion is stabilized by a number of hydrogen bonding interactions. The coordinated oxygen atom O2 interacts with the bridging solvent ligand W1 and the amido group of Asn 75. The most distant oxygen from the Mn(II) ions, O1, is hydrogen bonded to the ϵ nitrogen of His 76 and to W3 and is linked to Arg 53 and Asn 96 via an intervening water molecule (Figure 3b). His 76 is anchored in place by a salt bridge between its δ nitrogen and a side chain oxygen of Asp 52. This histidine residue, which corresponds to His 125 in PP1 (*16*), His 151 in bovine calcineurin (*18*), and His 202 in kidney bean PAP (*24*), has been proposed to play a key role in the catalytic mechanism (*29*). O3 interacts with W1, W3, and Arg 162, and O4 is connected to Asn 96 by a water molecule.

In molecule C, the sulfate ion is coordinated to both Mn1 and Mn2 in a monoatomic, bridging fashion (Figure 4). Although W2 remains and is still interacting with Asp 202, both W1 and W3 are displaced, and a single sulfate oxygen atom bridges the cluster with Mn···O1 distances of 2.1 and 2.4 Å. In addition, O2 is within bonding distance of Mn2, and O3 interacts weakly with Mn1 (Table 2). This sulfate adduct differs from the tungstate complex of PP1 (*17*) and the phosphate complex of calcineurin (*18*), both of which have the oxoanion coordinated to the two metal ions in a bidentate, bridging mode. The solvent ligand W2 remains in the same position as do all the protein ligands. The sulfate oxygen atoms interact with the same residues as in molecules A and B. O3 is hydrogen bonded to the ϵ nitrogen of His 76 and the ϵ nitrogen of Arg 53, and O2 interacts with Asn 75, His 76, and a water molecule that is linked to Asn 96 (Figure 4b). O4 is hydrogen bonded to Arg 162. The only residue that shifts position significantly is Arg 53. In molecules A and B, Arg 53 is connected to the bound sulfate ion through a water molecule, but in molecule C, the Cα atom has shifted ∼1 Å toward the dimanganese cluster, allowing a direct interaction with the sulfate oxygens (Figure 5). In addition to the strong interaction between the Arg 53 ϵ nitrogen and O3, both O3 and O4 are within 3.3 Å of the Arg 53 side chain ζ nitrogen.

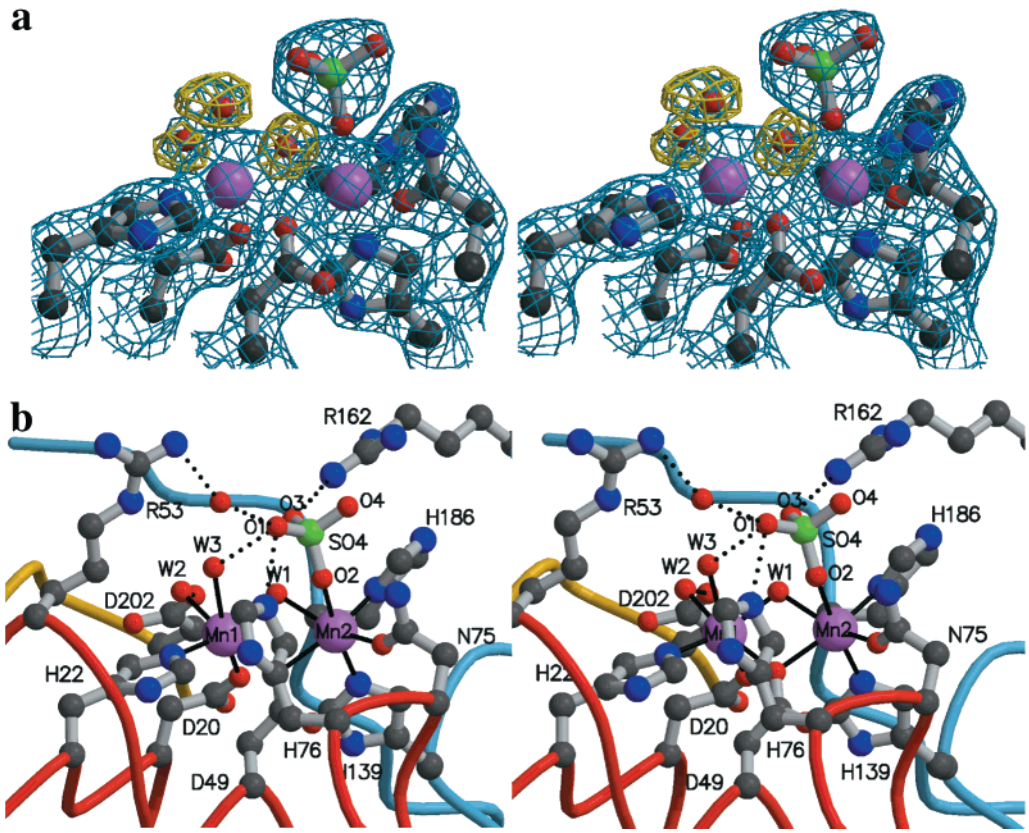

FIGURE 3: Active site with terminally bound sulfate ion (molecule A is shown; molecule B is very similar). (a) Stereoview of the final 2.15 Å resolution $2F_o - F_c$ electron density map at the dimanganese cluster (blue, contoured at 1.4σ). The $F_o - F_c$ map showing the coordinated and bridging solvent molecules is superimposed (yellow, contoured at 4σ). (b) Stereoview of the active site shown in the same orientation as in panel a. The backbone is shown in the same colors as in Figure 1. Bonds to the Mn(II) ions are denoted with solid black lines, and key hydrogen bonding interactions are highlighted with dotted black lines.

Comparison of the Three Independent Molecules. The overall structures of the three molecules in the asymmetric unit are very similar. Superpositions of the Cα atoms of molecules A and C, B and C, and A and B give root mean square (rms) differences of 0.428, 0.379, and 0.425 Å, respectively. The only extended region that exhibits significant differences between the three molecules is helix αD and the loop connecting helices αC and αD, corresponding to residues 86−97. These residues are involved in crystal lattice contacts between molecules A and C. By contrast, the same residues in molecule B are facing a solvent channel. Slight differences are also observed for residues 152−155 because Val 153 from molecule A interacts with Tyr 106 from a symmetry-related molecule A. The positions of the manganese ligands and neighboring residues, including His 76, are conserved between the three molecules, with the exception of the sulfate ion and Arg 53 (Figure 5). The shifted position of Arg 53 in molecule C is due to a crystal packing interaction with Asn 170 from a symmetry equivalent of molecule B. The side chain ζ nitrogen of Arg 53 is hydrogen bonded to the side chain oxygen of Asn 170, and its carbonyl oxygen interacts with the Asn 170 side chain nitrogen.

EPR spectra of the exchange-coupled dinuclear $[Mn(II)]_2$ cluster in the presence versus absence of sulfate are indistinguishable in terms of shape, temperature dependence, and power saturation behavior (data not shown), indicating that the exchange coupling is the same in both forms. By contrast, a weaker exchange interaction results when anion inhibitors such as phosphate, molybdate, and arsenate bridge the dinuclear iron centers of purple acid phosphatase (*51*) and calcineurin (*30*). These EPR data, combined with the observation that sulfate is a weak inhibitor (*22*), suggest that sulfate does not bridge the dimanganese cluster in solution, although it could bind in the terminal mode. Thus, the Arg 53 position in molecule C, which is due to the interactions described above, may stabilize the bridging coordination mode of the sulfate ion in the crystal. Although a bidentate coordination geometry could be accommodated without rearrangement of the active site residues, the position of Arg 53 apparently favors the tridentate coordination mode.

The most notable difference between the three molecules aside from the active site is the presence of ethylmercury derived from EMTS in molecules A and B (Figure 2) but not in molecule C. Well-defined electron density was observed for the mercury ion and its ethyl tail in both molecules A and B close to Cys 208. No extra electron density is observed at this position in molecule C. In molecule C, Phe 207 adopts a different rotamer from that observed in molecules A and B (Figure 5), possibly explaining the absence of bound mercury. Because of interactions with Lys 191 from a symmetry-related molecule C and Ile 172 from a neighboring molecule B, the Phe 207 phenyl ring is ∼6 Å closer to the active site and covers part of the substrate binding groove. This shift of Phe 207 completely exposes the sulfhydryl group of Cys 208. One explanation for the absence of mercury in molecule C is that the competitor thiol ligand DTT, present at 20 mM in the crystallization solution, removed mercury from this more accessible site by competing for ligation of the mercury ion.

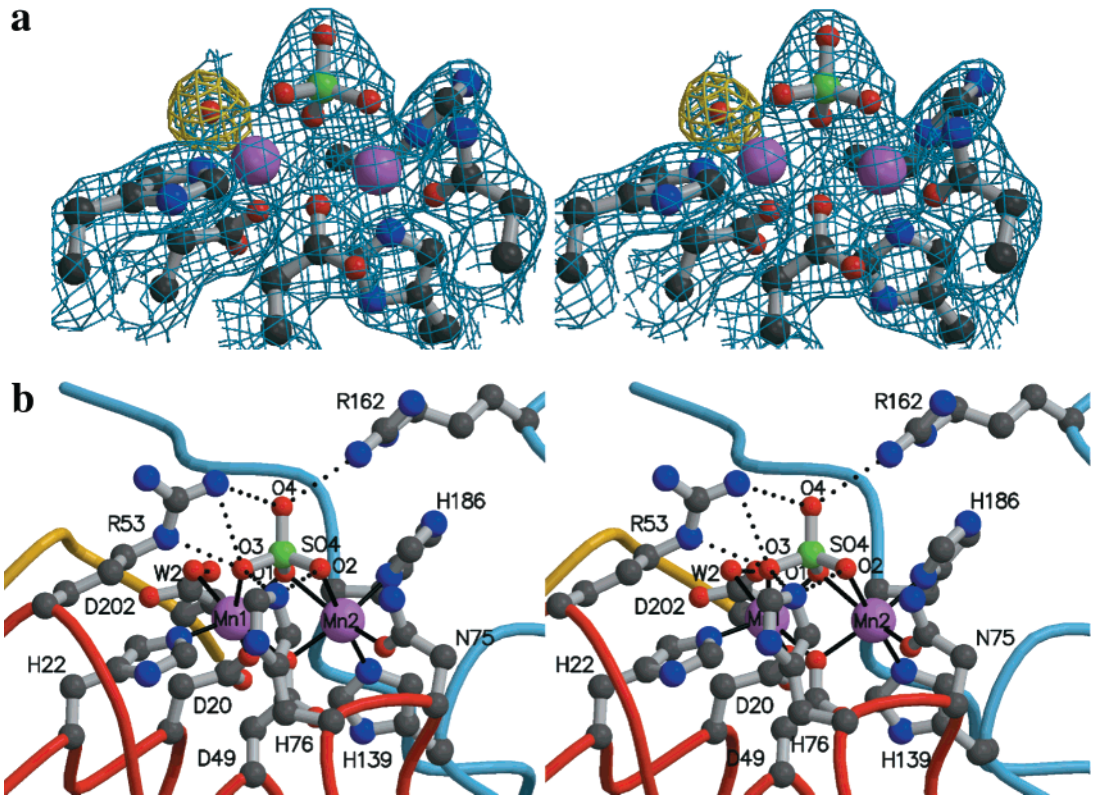

FIGURE 4: Active site with bridging sulfate ion (molecule C). (a) Stereoview of the final 2.15 Å resolution $2F_o - F_c$ electron density map at the dimanganese cluster (blue, contoured at 1.4σ). The $F_o - F_c$ map showing the solvent molecule coordinated to Mn1 is superimposed (yellow, contoured at 4σ). (b) Stereoview of the active site shown in the same orientation as in panel a. The backbone is shown in the same colors as in Figure 1. Bonds to the Mn(II) ions are denoted with solid black lines, and key hydrogen bonding interactions are highlighted with dotted black lines.

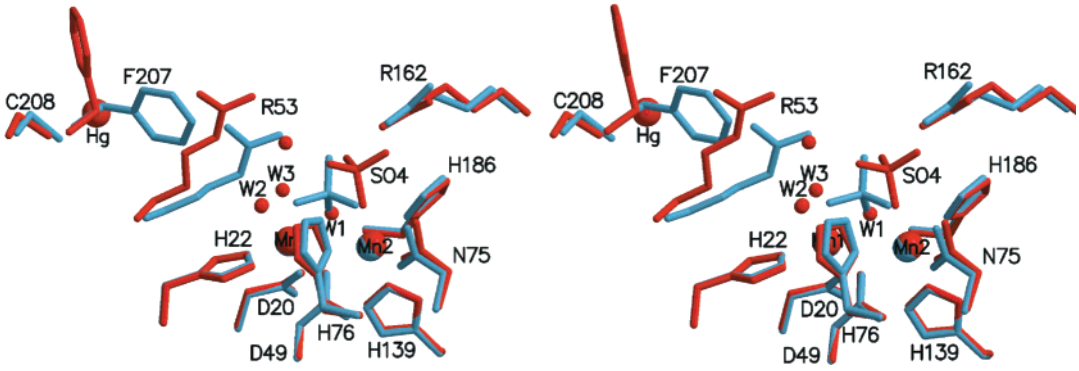

FIGURE 5: Stereo superposition of the active site and Hg(II) binding site in molecules A (red) and C (blue). The Hg(II) ion is only present in molecule A.

Implications for the Catalytic Mechanism of Ser/Thr PPases. The two arrangements of the λPP active site revealed by the structure provide models for intermediates that might occur during phosphoester hydrolysis. The dimanganese cluster with sulfate ion bound in a terminal, monodentate mode (Figure 3) is a good model for the initial complex formed upon binding of phosphorylated substrate to the active site. In the mechanism proposed in Figure 6, which is somewhat similar to mechanisms previously suggested for Ser/Thr PPases and PAPs (*8*, *15*, *17*, *24*), nucleophilic addition by a metal-coordinated solvent molecule to the phosphorus atom results in transfer of the phosphoryl group to the metal center. The dimanganese cluster with sulfate ion bound in a bridging mode (Figure 4) may represent a subsequent reaction intermediate in which the phosphoryl group has been transferred to the metal center following departure of the leaving group and a ligand exchange reaction involving substitution of one of the metal coordinated solvent molecules with a phosphate oxygen atom. Alternatively, it may represent a product-inhibited state. Displacement of the product phosphate by solvent exchange then returns the enzyme to the resting state.

Several lines of evidence support such a direct transfer mechanism. Isotope labeling studies on PAP (*52*) and kinetic and solvent isotope effect data for calcineurin (*53*, *54*) and λPP (*55*) are consistent with a single step reaction involving direct transfer of the phosphoryl group to a metal-coordinated solvent molecule. The identity of the nucleophilic solvent molecule (i.e., bridging versus terminal) has not been established however. One postulated role for the metal ions in Ser/Thr PPases is to activate this solvent molecule by lowering its pK_a (*8*, *15*, *56*, *57*). The bridging solvent ligand

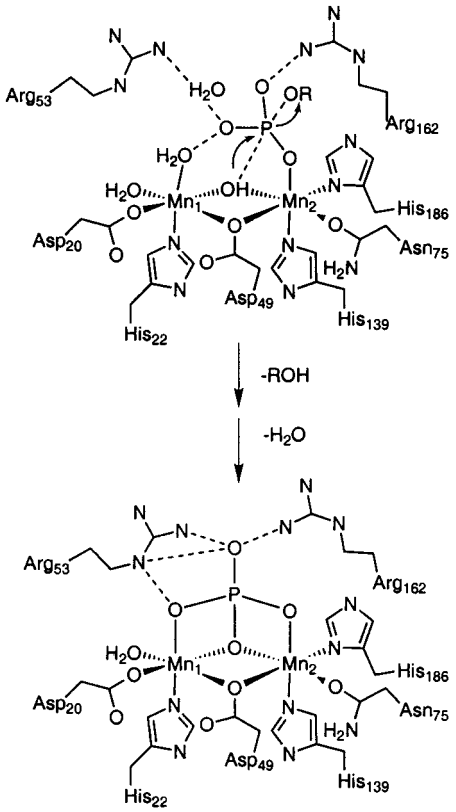

FIGURE 6: Proposed catalytic mechanism for phosphate ester hydrolysis by λPP and related Ser/Thr PPases using line drawings of the two crystallographically independent active site structures. A terminal water molecule coordinated to Mn1 could also act as the nucleophile.

in λPP, W1 (Figure 3), should have the lowest pK_a of the active site solvent molecules and is therefore the easiest to deprotonate to form hydroxide, the presumed nucleophile. Although structures of PP1 and calcineurin are available in the presence of anion inhibitors (*17*, *18*), the active site in λPP molecules A and B is the only Ser/Thr PPase structure in which an anion inhibitor and a bridging solvent molecule are bound simultaneously. As such, it is consistent with the bridging ligand serving as the attacking nucleophile. Additional support derives from oxygen isotope labeling studies of phosphate diester hydrolysis by a dicobalt(III) model compound (*58*). Nevertheless, the identity of the attacking nucleophile remains an open question.

Roles of Conserved Residues. Several residues from the phosphoesterase motif are believed to play important roles in the catalytic mechanism of Ser/Thr PPases. One such residue, His 76 in λPP or His 125/His 151 in PP1/calcineurin, has been widely proposed to act as a general acid catalyst, protonating the leaving group. Mutation of this histidine in both λPP and calcineurin results in a loss of activity (*14*, *29*), and the structures reveal that it is well positioned to protonate the leaving group (Figure 3b) (*16*−*18*, *24*). A comparison of k_{cat} values for substrates with leaving groups of different pK_a values suggests, however, that this residue is not required for protonation of the leaving group (*29*). In addition, kinetic isotope effects and pH rate profiles determined for the λPP variant in which His 76 is mutated to Asn do not provide definitive evidence for a general acid function (*55*). Protonation of the leaving group might instead be accomplished by the terminally bound solvent molecule W3, which like His 76, is hydrogen bonded to the O1 oxygen of the sulfate ion (Figure 3b). An alternative role proposed for His 76 is that of a general base, deprotonating the nucleophilic solvent molecule (*29*). Although the side chain of His 76 is not within hydrogen bonding distance of any of the coordinated solvent molecules in the two structures of λPP with bound sulfate, it is still possible it could interact with a metal-coordinated solvent molecule in the pre-Michaelis complex as it does in the structure of calcineurin (*19*). Nevertheless, it does interact with the sulfate oxygens in both coordination modes (Figures 3b and 4b), suggesting a likely role in both substrate positioning and stabilization of the transition state.

Another highly conserved residue is Arg 53 or Arg 96/Arg 122 in PP1/calcineurin. This arginine adopts a different conformation in molecule C than in molecules A and B (Figure 5). Mutation of λPP Arg 53 to alanine results in a substantial decrease in k_{cat} with little effect on substrate K_m, indicating an important role in catalysis. In addition, the IC_{50} for phosphate is increased for the mutant protein (*14*). As noted above, the change in coordination mode of the sulfate ion from terminal in molecules A and B to bridging in molecule C is associated with a shift in Arg 53. The direct interaction between Arg 53 and the sulfate oxygen atoms apparently stabilizes the sulfate in the bridging position, suggesting a possible role in transition state stabilization rather than binding and orienting the substrate prior to hydrolysis. This role is consistent with the observed increase in phosphate IC_{50} upon mutation of Arg 53 (*14*) since phosphate inhibition likely occurs by bridging the dimanganese cluster.

A second arginine in the active site, Arg 162, also interacts with the sulfate oxygens. This residue is not part of the phosphoesterase motif, but its presence in the active site is predicted by multiple sequence alignments of prokaryotic PPases (*59*). A similar interaction is observed in PP1 with Arg 221 (*17*) and calcineurin with Arg 254 (*18*), but these arginines are derived from structural elements not conserved in λPP. Mutation of Arg 162 to alanine results in significantly lower values of k_{cat} (*59*). Unlike Arg 53, Arg 162 interacts directly with the terminally bound sulfate ion in molecules A and B and shifts very little when the sulfate ion becomes bridging in molecule C. These findings suggest that Arg 162 might play a role in substrate recognition and positioning. Structural characterization of λPP in complex with substrates or inhibitors is required to further delineate the role of this arginine and other active site and surface groove residues in both substrate recognition and catalysis. Nevertheless, the λPP structure presented here provides both new insight into the mechanism of phosphoester hydrolysis by Ser/Thr PPases and a framework for interpretation of future mechanistic studies using λPP as a model system.

ACKNOWLEDGMENT

We thank N. Khidekel for assistance with crystallization, S. Garman and A. Lamb for helpful crystallographic discussions, and R. Lieberman for assistance with figure preparation. We also thank J. Quintana and D. Keane for assistance with data collection. The DND-CAT

Synchrotron Research Center at the Advanced Photon Source is supported by the E.I. DuPont de Nemours & Co., The Dow Chemical Company, the NSF, and the State of Illinois.

REFERENCES

1. Hunter, T. (1995) *Cell 80*, 225−236.
2. Kennelly, P. J., and Potts, M. (1996) *J. Bacteriol. 178*, 4759−4764.
3. Johnson, L. N., Noble, M. E. M., and Owen, D. J. (1996) *Cell 85*, 149−158.
4. Shi, L., Potts, M., and Kennelly, P. J. (1998) *FEMS Microbiol. Rev. 22*, 229−253.
5. Barford, D., Das, A. K., and Egloff, M.-P. (1998) *Annu. Rev. Biophys. Biomol. Struct. 27*, 133−164.
6. Denu, J. M., Stuckey, J. A., Saper, M. A., and Dixon, J. E. (1996) *Cell 87*, 361−364.
7. Fauman, E. B., and Saper, M. A. (1996) *Trends Biochem. Sci. 21*, 413−417.
8. Barford, D. (1996) *Trends Biochem. Sci. 21*, 407−412.
9. Shenolikar, S., and Nairn, A. C. (1991) *Adv. Second Messenger Phosphoprotein Res. 23*, 3−121.
10. DePaoli-Roach, A. A., Park, I.-K., Cerovsky, V., Csortos, C., Durbin, S. D., Kuntz, M. J., Sitikov, A., Tang, P. M., Verin, A., and Zolnierowicz, S. (1994) *Adv. Enzyme Regul. 34*, 199−224.
11. Rusnak, F., and Mertz, P. (2000) *Physiol. Rev. 80*, 1483−1521.
12. Cohen, P. T. W. (1994) *Adv. Protein Phosphatases 8*, 371−376.
13. Koonin, E. V. (1994) *Protein Sci. 3*, 356−358.
14. Zhuo, S., Clemens, J. C., Stone, R. L., and Dixon, J. E. (1994) *J. Biol. Chem. 269*, 26234−26238.
15. Rusnak, F., Yu, L., and Mertz, P. (1996) *J. Biol. Inorg. Chem. 1*, 388−396.
16. Goldberg, J., Huang, H.-b., Kwon, Y.-g., Greengrad, P., Nairn, A. C., and Kuriyan, J. (1995) *Nature 376*, 745−753.
17. Egloff, M.-P., Cohen, P. T. W., Reinemer, P., and Barford, D. (1995) *J. Mol. Biol. 254*, 942−959.
18. Griffith, J. P., Kim, J. L., Kim, E. E., Sintchak, M. D., Thomson, J. A., Fitzgibbon, M. J., Fleming, M. A., Caron, P. R., Hsiao, K., and Navia, M. A. (1995) *Cell 82*, 507−522.
19. Kissinger, C. R., Parge, H. E., Knighton, D. R., Lewis, C. T., Pelletier, L. A., Tempczyk, A., Kalish, V. J., Tucker, K. D., Showalter, R. E., Moomaw, E. W., Gastinel, L. N., Habuka, N., Chen, X., Maldonado, F., Barker, J. E., Bacquet, R., and Villafranca, J. E. (1995) *Nature 378*, 641−644.
20. Lohse, D. L., Denu, J. M., and Dixon, J. E. (1995) *Structure 3*, 987−990.
21. Klabunde, T., and Krebs, B. (1997) *Struct. Bonding 89*, 177−198.
22. Zhuo, S., Clemens, J. C., Hakes, D. J., Barford, D., and Dixon, J. E. (1993) *J. Biol. Chem. 268*, 17754−17761.
23. Sträter, N., Klabunde, T., Tucker, P., Witzel, H., and Krebs, B. (1995) *Science 268*, 1489−1492.
24. Klabunde, T., Sträter, N., Fröhlich, R., Witzel, H., and Krebs, B. (1996) *J. Mol. Biol. 259*, 737−748.
25. Guddat, L. W., McAlpine, A. S., Hume, D., Hamilton, S., de Jersey, J., and Martin, J. L. (1999) *Structure 7*, 757−767.
26. Uppenberg, J., Lindqvist, F., Svensson, C., Ek-Rylander, B., and Andersson, G. (1999) *J. Mol. Biol. 290*, 201−211.
27. Cohen, P. T. W., and Cohen, P. (1989) *Biochem. J. 260*, 931−934.
28. Rusnak, F., Yu, L., Todorovic, S., and Mertz, P. (1999) *Biochemistry 38*, 6943−6952.
29. Mertz, P., Yu, L., Sikkink, R., and Rusnak, F. (1997) *J. Biol. Chem. 272*, 21296−21302.
30. Yu, L., Golbeck, J., Yao, J., and Rusnak, F. (1997) *Biochemistry 36*, 10727−10734.
31. Huang, H.-B., Horiuchi, A., Goldberg, J., Greengard, P., and Nairn, A. C. (1997) *Proc. Natl. Acad. Sci. U.S.A. 94*, 3530−3535.
32. Zhang, J., Zhang, Z., Brew, K., and Lee, E. Y. C. (1996) *Biochemistry 35*, 6276−6282.
33. Mackintosh, C., and Mackintosh, R. W. (1994) *Trends Biochem. Sci. 19*, 444−448.
34. Tabor, S., and Richardson, C. C. (1985) *Proc. Natl. Acad. Sci. U.S.A. 82*, 1074−1078.
35. Otwinowski, Z., and Minor, W. (1997) *Methods Enzymol. 276*, 307−326.
36. Collaborative Computational Project, N. (1994) *Acta Crystallogr. D50*, 760−763.
37. Sheldrick, G. M., and Schneider, T. R. (1997) *Methods Enzymol. 277*, 319−343.
38. Brünger, A. T., Adams, P. D., Clore, G. M., DeLano, W. L., Gros, P., Grosse-Kunstleve, R. W., Jiang, J.-S., Kuszewski, J., Nilges, M., Pannu, N. S., Read, R. J., Rice, L. M., Simonson, T., and Warren, G. L. (1998) *Acta Crystallogr. D54*, 905−921.
39. Jones, T. A., Zou, J.-Y., Cowan, S. W., and Kjeldgaard, M. (1991) *Acta Crystallogr. A47*, 110−119.
40. Laskowski, R. A. (1993) *J. Appl. Crystallogr. 26*, 283−291.
41. Kraulis, P. J. (1991) *J. Appl. Crystallogr. 24*, 946−950.
42. Merritt, E. A., and Bacon, D. J. (1997) *Methods Enzymol. 277*, 505−524.
43. Nicholls, A., Sharp, K. A., and Honig, B. (1991) *Proteins 11*, 281−296.
44. Esnouf, R. M. (1997) *J. Mol. Graphics Modell. 15*, 132−134.
45. Solow, B., Young, J. C., and Kennelly, P. J. (1997) *J. Bacteriol. 179*, 5072−5075.
46. Holm, R. H., Kennepohl, P., and Solomon, E. I. (1996) *Chem. Rev. 96*, 2239−2314.
47. Weyhermüller, T., Weighardt, K., and Chaudhuri, P. (1998) *J. Chem. Soc., Dalton Trans. 22*, 3805−3813.
48. Yu, S.-B., Lippard, S. J., Shweky, I., and Bino, A. (1992) *Inorg. Chem. 31*, 3502−3504.
49. Bossek, U., Wieghardt, K., Nuber, B., and Weiss, J. (1989) *Inorg. Chim. Acta 165*, 123−129.
50. Khangulov, S. V., Sossong, T. M., Ash, D. E., and Dismukes, G. C. (1998) *Biochemistry 37*, 8539−8550.
51. David, S. S., and Que, L., Jr. (1990) *J. Am. Chem. Soc. 112*, 6455−6463.
52. Mueller, E. G., Crowder, M. W., Averill, B. A., and Knowles, J. R. (1993) *J. Am. Chem. Soc. 115*, 2974−2975.
53. Martin, B. L., and Graves, D. J. (1986) *J. Biol. Chem. 261*, 14545−14550.
54. Martin, B. L., and Graves, D. J. (1994) *Biochim. Biophys. Acta 1206*, 136−142.
55. Hoff, R. H., Mertz, P., Rusnak, F., and Hengge, A. C. (1999) *J. Am. Chem. Soc. 121*, 6382−6390.
56. Rusnak, F., Mertz, P., Reiter, T., and Yu, L. (1999) in *Iron metabolism: inorganic biochemistry and regulatory mechanisms* (Ferreira, G. C., Moura, J. J. G., and Franco, R., Eds.) pp 275−302, Wiley-VCH, Weinheim.
57. Rusnak, F. (2000) *Met. Ions Biol. Syst. 37*, 305−343.
58. Wahnon, D., Lebuis, A.-M., and Chin, J. (1995) *Angew. Chem., Int. Ed. Engl. 34*, 2412−2414.
59. White, D., Reiter, N., and Rusnak, F. Unpublished results.

BI0021030